An Ultrathin Self-Humidifying Membrane for PEM Fuel Cell Application: Fabrication, Characterization, and Experimental Analysis

Xiaobing Zhu,[†,‡] Huamin Zhang,[*,†] Yu Zhang,[†,‡] Yongmin Liang,[†,‡] Xiaoli Wang,[†,‡] and Baolian Yi[†]

Proton Exchange Membrane Fuel Cell Key Materials and Technology Laboratory, Dalian Institute of Chemical Physics, Chinese Academy of Sciences, 457 Zhongshan Road, Dalian 116023, China, and Graduate School of the Chinese Academy of Sciences, Beijing 100039, China

Received: March 29, 2006

An ultrathin poly(tetrafluoroethylene) (PTFE)-reinforced multilayer self-humidifying composite membrane (20 μm, thick) is developed. The membrane is composed of Nafion-impregnated porous PTFE composite as the central layer, and SiO_2 supported nanosized Pt particles ($Pt-SiO_2$) imbedded into the Nafion as the two side layers. The proton exchange membrane (PEM) fuel cell employing the self-humidifying membrane ($Pt-SiO_2$/NP) turns out a peak power density of 1.40 W cm^{-2} and an open circuit voltage (OCV) of 1.032 V under dry H_2/O_2 condition. The excellent performance is attributed to the combined result of both the accelerated water back-diffusion in the thin membrane and the adsorbing/releasing water properties of the $Pt-SiO_2$ catalyst in the side layers. Moreover, the inclusion of the hygroscopic $Pt-SiO_2$ catalyst inside the membrane results in an enhanced anode self-humidification capability and also the decreased cathode polarization (accordingly an improved cell OCV). Several techniques, such as transmission electronic microscopy, scanning electronic microscopy, energy dispersive spectroscopy, thermal analysis and electrochemical impedance spectroscopy etc., are employed to characterize the $Pt-SiO_2$/NP membrane. The results are discussed in comparison with the plain Nafion/PTFE membrane (NP). It is established that the reverse net water drag (from the cathode to the anode) across the $Pt-SiO_2$/NP membrane reaches 0.16 H_2O/H^+. This implies a good hydration of the $Pt-SiO_2$/NP membrane and thus ensures an excellent PEM fuel cell performance under self-humidification operation.

1. Introduction

Proton exchange membrane (PEM) fuel cells are promising alternative energy conversion devices for transportation and stationary applications due to their high energy conversion efficiency and environmental benefits.[1−7] Currently, the development of key materials, the PEMs and the electrocatalysts, is now considered as the impediment to the success of the PEM fuel cell technology and thus should be given high priority.[8−13] Nafion membranes (more than 50 μm in thickness) are extensively used as the polymer electrolytes for their good chemical and mechanical properties. In this case, the membrane proton conductivity almost linearly depends on water content of the membranes.[14−20] Usually, PEM fuel cells are operated at around 80 °C with H_2 and O_2 or air humidified prior to entry into the cells.[11] However, this external humidifying subsystem often introduces complexity to the system. Therefore, operation of PEM fuel cells without humidification subsystems can not only greatly facilitate water and thermal management but also reduce the system weight and complexity. [21−26]

To realize self-humidification operation of PEM fuel cells, most of the literature focuses on development of the functional PEMs, e.g., self-humidifying membranes. Watanabe et al.[27−30] proposed a concept of Nafion112-based self-humidifying membranes on the basis of suppressing mutual permeation of the reactant gases through the membranes. In their work, the membranes were prepared by uniformly incorporating nanometer-sized Pt (as water generation site) and hydrophilic inorganic oxides (as water retention sites) in Nafion112 membrane. Another concept of a self-humidifying membrane was developed by Lee et al.[31] The membrane was developed by impregnating nanometer-sized Pt crystallites into Nafion112 membrane by reducing $Pt(NH_3)_4^{2+}$, followed by in situ precipitation of zirconium phosphate in the Pt−Nafion membrane. However, the thus-prepared self-humidifying membranes could not be made thinner than 50 μm due to mechanical deficiency of the substrate membrane. Recently, Xing et al.[32] investigated a self-humidifying composite membrane based on sulfonated poly(ether ether ketone) (donated as SPEEK). The membrane was prepared by first casting SPEEK solution onto porous PTFE film to obtain SPEEK/PTFE as a base layer and then recasting the ink of SPEEK and Pt/C catalyst onto the SPEEK/PTFE base layer to form a Pt−C/SPEEK layer. Similarly, Yang et al.[33] studied a Nafion-based self-humidifying membrane, which was prepared by recasting the ink of Nafion and Pt/C catalyst to form a Pt/C−Nafion layer and hot-pressing together with pure Nafion membrane. Furthermore, Liu et al.[34] synthesized a self-humidifying Pt−C/Nafion/PTFE membrane by casting the ink of Nafion solution and Pt/C catalyst onto a porous PTFE film. In these synthesis methods, however, Pt/C particles were distributed in the membrane and may thus cause a short circuit of the membrane due to electronic conduction of Pt/C.

* To whom correspondence should be addressed. E-mail address: zhanghm@dicp.ac.cn. Tel.: +86-411-84379072. Fax: +86-411-84665057.

† Proton Exchange Membrane Fuel Cell Key Materials and Technology Laboratory, Dalian Institute of Chemical Physics, Chinese Academy of Sciences.

‡ Graduate School of the Chinese Academy of Sciences.

10.1021/jp061955s CCC: $33.50
Published on Web 07/06/2006

It is noteworthy that most of the self-humidifying membranes were prepared by imbedding the platinum and/or hygroscopic oxides in the membranes, and very few publications concern introducing hygroscopic oxides supported platinum catalysts in the membranes. The peak power density of the fuel cells employing these membranes is only as high as 0.6 W/cm^2 when they are operated under dry reactant gases. Tests on commercially available Gore-Select membranes (5−20 μm) indicate that not only the PTFE reinforcement could be an effective way for development of ultrathin PEMs but also the decreased membrane resistance of thin membranes can greatly improve cell performance. The back-diffusion of water to the anode is the dominant process in the distribution of water in the self-humidification fuel cell, and the rate of water back-diffusion must be sufficiently high so that the ionic conductivity is not significantly impaired.[36] Moreover, the net water transport phenomena (from the anode to the cathode) across the membrane under external-humidifying operation was predicted and observed,[19,35] and the reverse one (from the cathode to the anode) was only qualitatively implied under dry operation. [36,26] Interestingly, however, there are few quantificational reports on the reverse net water transport toward the anode, obtained through the optimized Pt−SiO_2/NP membrane structure in the self-humidifying membrane fuel cells under dry operation, especially under normal constant H_2 and O_2 stoichiometries ($\lambda_{H_2} = 1.1$ and $\lambda_{O_2} = 2$).

In this paper, we present an ultrathin PTFE-reinforced self-humidifying composite membrane (Pt−SiO_2/NP) with a sandwich structure, which is composed of a central layer and two side layers. The central layer was prepared by impregnating Nafion into a porous PTFE film to obtain a Nafion/PTFE layer, and the two side layers were obtained by spraying the ink of Nafion and silicon oxide supported platinum catalyst (Pt−SiO_2) onto the Nafion/PTFE layer. The designing sandwich structure of our Pt−SiO_2/NP membrane is based on acceleration of water back-diffusion resulting from an ultrathin membrane and suppression of reactant gases permeation arising from the thin Nafion/PTFE membrane (NP). The Pt−SiO_2/NP membrane was characterized by transmission electron microscopy (TEM), inductively coupled plasma-atomic emission spectroscopy (ICP-AES), scanning electron microscopy (SEM), energy dispersive spectroscopy (EDS), thermogravimetric analyzer (TGA), tension tester AG-2000A, and gas chromatograph measurements. Duplicate tests have shown that the single PEM fuel cell employing our Pt−SiO_2/NP membrane exhibited an excellent cell performance and also a high open circuit voltage (OCV) in the dry operation mode. To further confirm the surprising self-humidification property of our Pt−SiO_2/NP membrane, electrochemical impedance spectroscopy (EIS) measurements were conducted to obtain the areal resistance of both the Pt−SiO_2/NP membrane and the plain NP membrane in the PEM fuel cells under wet or dry operation modes. Furthermore, the collected water experiment was conducted to discuss the water balance inside the operating Pt−SiO_2/NP and NP membranes in detail.

2. Experimental Section

2.1. Fabrication of the Pt−SiO_2/NP and the NP Membranes. The Pt−SiO_2 catalyst was obtained by impregnation of silicon oxide (BET surface area of 112 m^2/g, average particle size of 20 nm, commercial product made in Japan) with aqueous solution of H_2PtCl_6 (3.7 mg of Pt/mL, A.P., Sino-Platinum Metals Co., Ltd.) for 24 h. The resulting mixture was dried at room temperature in air and reduced by H_2 at 200 °C for 3 h. The volumetric ratio of H_2PtCl_6 solution and SiO_2 was 1:1, and the Pt loading on SiO_2 was designed as 1 wt %.

The Pt−SiO_2/NP membrane was a sandwich structure. The central layer Nafion/PTFE was prepared by pouring 5 wt % modified Nafion solution onto a porous PTFE film (15 μm in thickness, 0.3−0.5 μm in pore diameter, ~ 85% in porosity, Dagong New Mater. Co., Shanghai, China). The pure Nafion resin was first obtained by evaporation of 5 wt % Nafion solution (Dupont Fluoroproducts, EW= 1100 g/mol SO_3H) at 100 °C under vacuum for 24 h until dry, then redissolved in a mixed solvent containing dimethyl sulfoxide (DMSO) and ethanol (volume ratio, 1:1) at 60 °C in a closed vessel to obtain the above-mentioned 5 wt % modified Nafion solution. The PTFE film was preliminarily extended on a stainless steel frame. The membrane was heated at 70−77 °C until dry, and treated at 120 °C for at least 10 h. The Pt−SiO_2 catalyst was dispersed in a solution of 5 wt % Nafion and isopropyl alcohol (IPA) to form a homogeneous ink. The ink was sprayed onto the two sides of the Nafion/PTFE layer, resulting in a layer of about 2.5 μm of thickness at each side. The mass ratio of the Nafion resin to the Pt−SiO_2 catalyst inside the two side layers was kept at 6:1, and hence the Pt−SiO_2 catalyst loading inside the Pt−SiO_2/NP membrane was designed to be 1.7×10^{-1} mg/cm^2. The three-layer membrane was about ca. 20 μm in thickness and allowed to dry in air. For comparison, a plain NP membrane without Pt−SiO_2 catalyst was prepared by the same way. The thickness of the NP membrane was also about ca. 20 μm. The thickness of the composite membranes can be easily adjusted by changing the amounts of the Nafion solution and the Pt−SiO_2 catalyst[34] and was determined by electronic outside micrometers (resolution, 0.001 mm; Qinghai Measuring & Cutting Tools Co. Ltd., China).

2.2. Characterization of the Membranes. 2.2.1. Equivalent Weight (EW) Measurement. The ion content can be characterized by the molar equivalents of ion conductor per mass of dry membrane and expressed as EW with units of grams of dry membrane per equivalent. The EW values of Pt−SiO_2/NP and NP membranes were determined by titration as follows.[37] One to two grams of the samples were placed in 0.5 M aqueous NaOH and allowed to remain undisturbed for 1 day. The solution was then back-titrated with 0.1 M HCl using phenolphthalein as an indicator.

2.2.2. TEM, ICP-AES, SEM, and EDS Analyses. TEM (JEM-2000EX, JEOL, Japan) micorgraphs were taken on Pt−SiO_2 catalyst and SiO_2 particle. The samples were dispersed in ethanol, using an ultrasonic bath, and then mounted on standard copper TEM grids. ICP-AES (Plasma-Spec-II, LEEMAN Inc., USA) analysis of the Pt−SiO_2 catalyst was conducted to determine the bulk content of Pt. The surface and the cross-sectional morphology of the Pt−SiO_2/NP and the NP membranes were investigated by SEM (JEOL 6360LV, Japan). The distributions of fluorine, sulfur, and silicon elements along the membrane cross section were detected by EDS (Oxford Instruments Microanalysis 1350).

2.2.3. Water Content of the Membranes. The membrane samples were pretreated by the following procedure: boiling in 3% hydrogen peroxide, rinsing in boiling water, boiling in 0.5 M sulfuric acid, and finally rinsing in boiling water (1 h for each step).[19] To determine total water content, the above-pretreated membranes were removed from liquid water, blotted dry to remove the excess surface water, and quickly weighed in a closed vessel. The membrane samples were dried at 105 °C for 10 h under vacuum, and the total water content was determined from the difference between wet and dry weights.[19] For measurement of the bound water content, the above-pretreated samples were heated in a high-resolution thermo-

gravimetric analyzer (TGA, PerkinElmer Instruments) at a rate of 10 °C min^{-1} from 30 to 200 °C with nitrogen as carrier gas. The weight loss percentage of the membranes in the temperature ranging from 100 to 150 °C, which indicates the bound water content, was recorded.[38] The bound water content was obtained by subtracting the dry weight at 150 °C from the wet weight at 100 °C.

2.2.4. Mechanical Strength, Dimensional Stability, and H_2/O_2 Permeability of the Membranes. The membrane mechanical properties were measured by a tension tester AG-2000A (Shimadzu, AUTO graph) at room temperature, in accordance with China Standard QB-13022-91. Membrane specimens were tested using a programmed elongation rate of 50 mm min^{-1}.

All the membranes should be in H^+-form PEMs and kept dry by filter paper for at least 1 week before using. The distance between the specified positions of the membrane samples was measured before and after the samples were boiled in deionized (DI) water for 30 min. Then, the dimensional change of membranes (ΔL) was calculated by eq 1

$$\Delta L = \frac{L_2 - L_1}{L_1} \times 100\% \quad (1)$$

where L_1 and L_2 mean the distance before and after the samples were boiled in DI water, respectively.

The hydrogen and oxygen permeability of the membranes was measured by a gas chromatographic method using nitrogen and helium as carrier gases, respectively.[39]

2.3. Self-Humidification Effect of the Pt−SiO_2/NP Membrane. 2.3.1 Single PEM Fuel Cell Tests. The membrane electrode assemblies (MEAs) were fabricated by hot-pressing the anode and the cathode to the membrane at 140 °C and 10 MPa for 2 min. The Pt loadings in the anode and the cathode were 0.3 and 0.5 mg/cm^2, respectively. The Nafion loadings in both the anode and the cathode were 0.4 mg/cm^2. The active area of MEAs was 5 cm^2. The MEA was placed in a single cell using stainless steel as the end plates and stainless mesh as the current collectors.

To check the self-humidifying effect of the Pt−SiO_2/NP membrane, the single cell was kept running with dry H_2 and O_2. After stable cell performance was maintained for 8 h, the cell voltages at different current densities were recorded. The single cell with the Pt−SiO_2/NP membrane was evaluated at various temperatures under dry and wet operation modes. For comparison, the cell employing the NP membrane was operated at the same temperature under dry conditions.

2.3.2. Resistance Measurement. EIS measurements were carried out to obtain the areal resistance of the Pt−SiO_2/NP membrane under wet and dry operation modes and also that of the plain NP membrane under dry operation. A frequency response detector (EG&G model 1025, Princeton Applied Institute) and a potentiostat/galvanostat (EG&G model 273A, Princeton Applied Institute) were employed for the measurements.

2.3.3. Water Collection at the Anode and the Cathode. The net water transport across an operating fuel cell under dry operation was measured by collecting water at the anode and the cathode outlets by ice trap.[19,28] Before the collection of water, the cells were operated under steady state (constant current and fluxes) conditions for 8 h. Then the outlet gases were switched toward the ice trap to start water collection. During the collection of water, the cells were operated for 8 h under the same conditions. After the collection time was completed, the outlet gases were switched off. Water that remained in the gas tubes was blown into the ice traps with dry N_2. By such a procedure, the collected water in the ice trap was guaranteed to be that obtained in the course of the collection time.

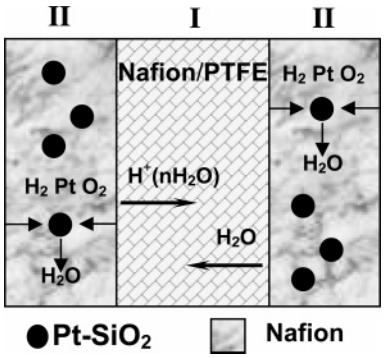

Figure 1. Schematic diagram of Pt−SiO_2/NP membrane with sandwich structure: (I) Nafion/PTFE, central layer; (II) Pt−SiO_2/Nafion, side layers.

3. Results and Discussion

3.1. Self-Humidification Mechanism of the Pt−SiO_2/NP Membrane. It is well-known that Nafion family membranes have microporous structure.[40] This can result in the mutual permeation of reactant gases and lead to mixed potential and remarkable polarization at the cathode. In addition, the self-humidification at the anode side is of importance [32−34] because the membrane specific resistance (ρ) of the anode side is larger than that of cathode side under dry operation.[29] Springer et al. predicted an increase in membrane resistance with increased current density and demonstrated a great advantage of a thinner membrane in alleviating the membrane resistance problem.[35]

Figure 1 demonstrates the sandwich structure of our ultrathin Pt−SiO_2/NP membrane. The Pt−SiO_2/NP membrane was designed to be a sandwich structure on the two considerations. One is that water back-diffusion from the cathode to the anode could be accelerated by the ultrathin membrane. The other is that the permeation of the reactant gases arising from the thin NP membrane could be suppressed by the Pt−SiO_2 catalyst particles in the two side layers. However, the crucial issue here is how to keep water balance in the operating membrane. The central layer, Nafion/PTFE reinforced composite membrane, allows ultrathin membrane feasible to be employed in PEM fuel cell. The reduction in membrane thickness can accelerate the crossover of H_2 and O_2 and facilitate water back-diffusion. In fact, hydrophilic nanometer-sized SiO_2 inside the membrane is expected to adsorb water at low current density and to release water at high current density to satisfy the electro-osmotic drag requirement.[30]

In the work of Watanabe et al.,[41] the anode polarization reached 20 mV vs reversible hydrogen electrode (RHE) at 50 A/cm^2 under an electrochemically controlled condition with fully utilized Pt particle surface, indicating negligible H_2 electrode polarization property. However, traces of H_2 permeating from the anode to the cathode reacted with O_2 on Pt catalyst surface to form H_2O at the cathode side. Thus a generated short circuit current could produce a mixed potential and cause a remarkable O_2 electrode polarization even at low current density.[29] The Pt−SiO_2 catalyst in both side layers suppresses gas crossover by chemically catalyzing mutually permeable H_2 and O_2 to produce H_2O, which can in situ hydrate the Pt−SiO_2/NP membrane and facilitate water balance.

Therefore, in our design, the anode side layer was used for membrane self-humidification and the cathode side layer aims

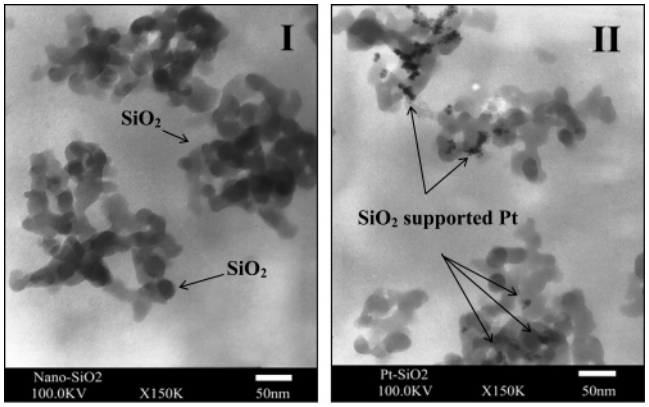

Figure 2. TEM images of nanometer-sized (I) SiO_2 particle and (II) $Pt-SiO_2$ catalyst particle.

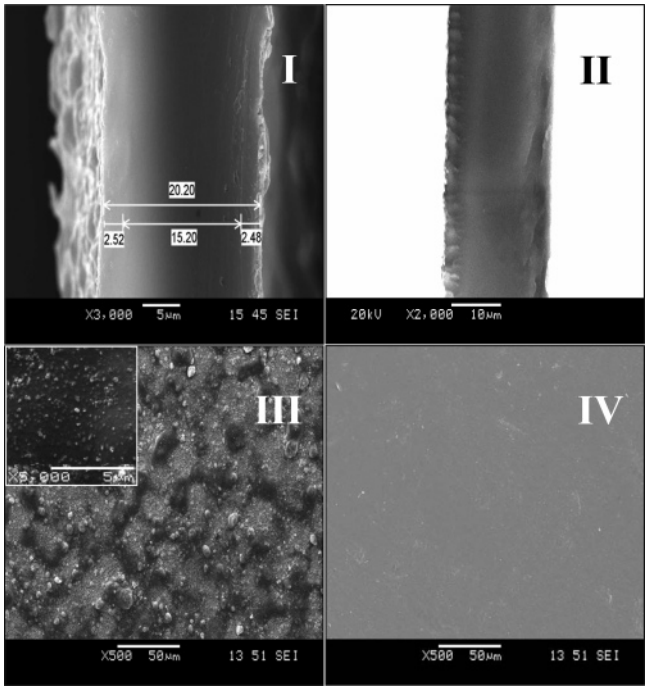

Figure 3. SEM images of the $Pt-SiO_2$/NP (I, III) and NP (II, IV) membranes. I and II represent membrane cross sections. III and IV represent membrane surfaces. Both membrane thickness values are 20 μm.

to decrease oxygen electrode polarization, especially at low current density, and accordingly improve the cell OCV.

3.2. Characterizations of the Membranes. 3.2.1. TEM, ICP-AES, SEM, and EDS Analyses. Figure 2 shows the TEM images of silicon oxide and $Pt-SiO_2$ catalyst. The Pt particles are sparsely dispersed on the support due to the low Pt loading with a size of 2−4 nm. The diameters of SiO_2 and $Pt-SiO_2$ particles are about 20 nm. The $Pt-SiO_2$ powder loading inside our $Pt-SiO_2$/NP membrane was 0.17 mg/cm^2, which is comparable to 0.1 mg/cm^2 of Pt/C catalyst (20 wt % Pt on carbon) loading in the Nafion-based self-humidifying membrane prepared by Yang et al.[33] ICP-AES analysis showed that the bulk Pt content in the $Pt-SiO_2$ catalyst was 0.93 wt %. The calculation turned out a Pt loading of 1.6×10^{-3} mg/cm^2 inside our $Pt-SiO_2$/NP membrane.

To investigate membrane surface and cross-sectional morphology, SEM measurements were conducted. The cross-sectional morphology of the $Pt-SiO_2$/NP membrane is apparently composed of three layers (Figure 3 I), as compared to that of the plain NP membrane (Figure 3 II). The anode side

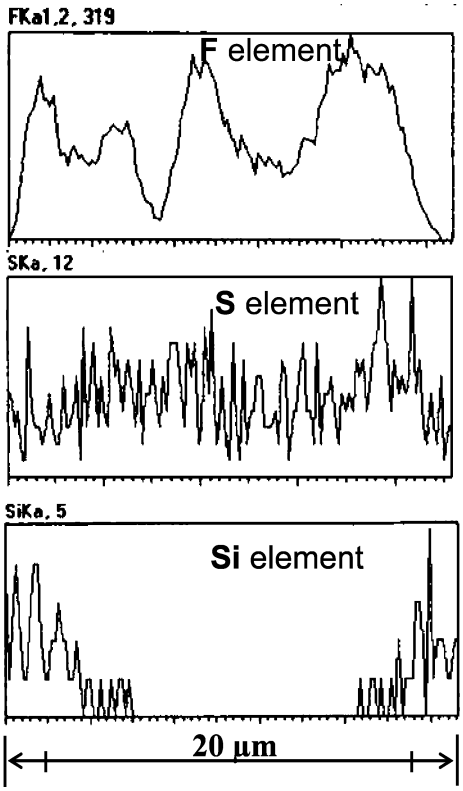

Figure 4. EDS elements analysis along cross-sectional $Pt-SiO_2$/NP membrane.

layer and the cathode side layer are located at both sides of the Nafion/PTFE central layer. It can be clearly seen that the inorganic catalyst particles located in both side layers are completely separated by the central Nafion/PTFE layer, thus avoiding microphase separation in the whole membrane and ensuring the feasibility of high cell OCV. In addition, panels III and IV of Figure 3 reveal a rough surface on the $Pt-SiO_2$/NP membrane due to the existence of $Pt-SiO_2$ catalyst particles, in contrast to a smooth surface of the plain NP membrane. The rough membrane surface could enlarge the interface area between the membrane and the electrodes.

Figure 4 and Figure 5 show the EDS results of the $Pt-SiO_2$/NP membrane and the NP membrane, respectively. The elemental analysis on the cross section of the membranes facilitates the understanding of the composite membrane structure. For the $Pt-SiO_2$/NP membrane, it is observed that the fluorine content is lower in the two side layers and nonhomogeneous in the central layer. The lower content of fluorine in the two side layers is due to the lower Nafion content in these layers. On the other hand, hygroscopic SiO_2 particles can easily bond to the hydrophilic SO_3H- groups in the Nafion membrane. It has been established that for Nafion membranes, the fluorine element usually locates in the hydrophobic domains, while the SO_3H- groups usually locate in the hydrophilic domains.[42] Therefore, during our preparation of the membrane, some SiO_2 particles may invade into the central layer and the nonhomogeous distribution of the SiO_2 particles in the central layer may lead to the nonhomogeneous distribution of fluorine. As for the NP membrane, in accordance with the existence of a fluorine-rich region near the surface in the Nafion membrane,[42] the fluorine content is larger in the near-surface part than in the central part.

From Figure 4 and Figure 5, it also can be seen that the sulfur (S) element is uniformly distributed along the cross-sectional direction in these two membranes. This manifests that the Nafion

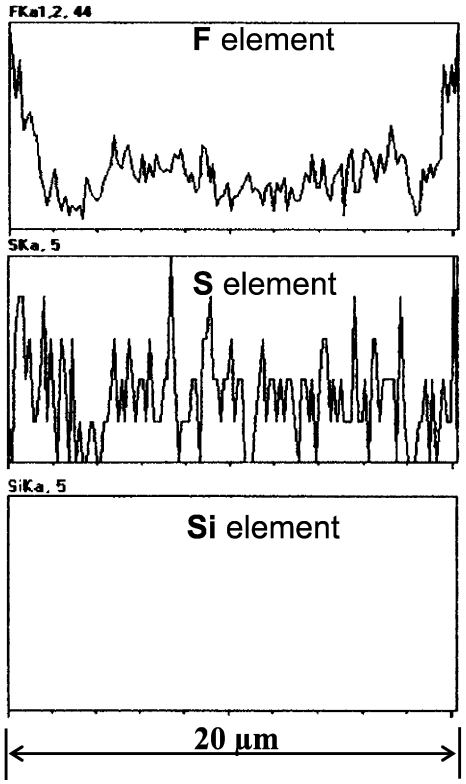

Figure 5. EDS elements analysis along cross-sectional NP membrane.

resin has been homogeneously impregnated into the porous PTFE film. The characteristic silicon (Si) element is distributed at the two side layers of the Pt−SiO_2/NP membrane due to the existence of the Pt−SiO_2 catalyst. Since the Pt loading in the Pt−SiO_2/NP membrane was too low to be analyzed quantitatively, the Pt element distribution was not given here.

3.2.2. Water Content of the Membranes. There are two different types of water in PEMs.[40] One type of water is needed for the solvation of the sulfonic groups and the other type of water fills the micropores and behaves like bulk water. For the sake of simplicity, the two kinds of distinguished water are defined as the bound water and the bulk water. The total water content and bound water content of the membranes are calculated according to eqs 2 and 3

$$\Delta W = \frac{W_{\text{wet}} - W_{\text{dry}}}{W_{\text{dry}}} \times 100\% \quad (2)$$

$$\lambda_{(H_2O/SO_3H)} = \frac{(W_{\text{wet}} - W_{\text{dry}})}{18 \times W_{\text{dry}}} \times \text{EW} \quad (3)$$

where W_{wet} and W_{dry} represent the weight of the wet and dry membrane, respectively. ΔW and λ parameters represent the mass content of water uptake and water molecule number per SO_3H group of the membranes, respectively. Subtraction of the bound water content from the total water content gives the bulk water content. The EW value of Nafion112 membrane is obtained from the Dupont Company.

Figure 6 shows the bound water content of Pt−SiO_2/NP, NP, and Nafion112 membranes measured by TGA. For easy comparison of weight loss characteristics, the weight percentages of the three membrane samples at 100 °C were all fixed at 100%. As indicted in the Figure 6, the weight loss percentage (wt %)—namely, the bound water content, increases with the decreased EW values, e.g., 1300 and 1100 g/mol SO_3H of the NP and

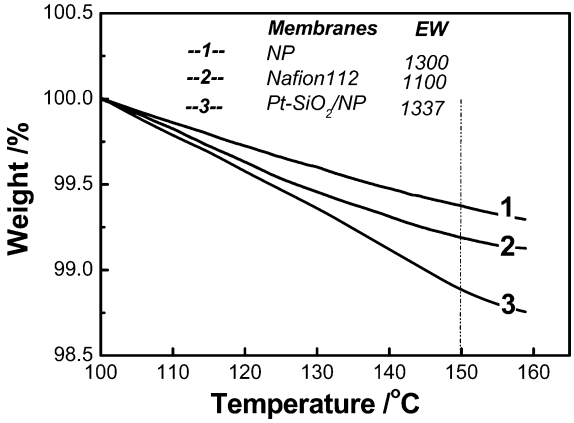

Figure 6. The bound water content comparison of the Pt−SiO_2/NP, NP, and Nafion112 membranes measured by TGA. The weight loss percentages of the membranes in the temperature ranging from 100 to 150 °C represent the bound water content.

Nafion112 membranes. However, the bound water content of the Pt−SiO_2/NP membrane with the highest EW (1337 g/mol SO_3H) was the largest among the membranes due to hygroscopic property of the Pt−SiO_2 catalyst in the membrane.

Table 1 compares the contents of total/bulk/bound water of the Pt−SiO_2/NP membrane, the NP membrane, and the Nafion112 membrane. Since λ and ΔW are related by a simple proportionality, the water content values of these membranes show very similar trends in λ and ΔW formations. It is found that the total/bulk/bound water contents of the NP and Nafion112 membranes increase with the decreased EW value. The total water content value of Nafion112 is 30.3% in ΔW formation, which is consistent with ref 43. However, the total/bulk/bound water content values of the Pt−SiO_2/NP membrane with the highest EW value are the largest due to water adsorbing ability of the Pt−SiO_2 catalyst. It should be noted that the total/bulk/bound water contents of the Pt−SiO_2/NP membrane are 40.5/39.6/0.9 H_2O/SO_3H (in λ formation) and 54.5/53.3/1.2 wt % (in ΔW formation), respectively, which is almost twice those of the NP membrane. The high water content in the Pt−SiO_2/NP membrane is attributed to the hygroscopic property of Pt−SiO_2 catalyst and facilitates water balance in the membrane, which in turn contributes to the good single fuel cell performance.

3.2.3. Mechanical Strength, Dimensional Stability, and H_2/O_2 Permeability of the Membranes. Table 2 presents the mechanical properties, the dimensional stability, and the oxygen and hydrogen permeability properties of the Pt−SiO_2/NP, NP, and Nafion112 membranes. The Pt−SiO_2/NP and NP membranes exhibit much larger mechanical strength, e.g., maximum strength and break strength, and lower dimensional change values due to the PTFE reinforcement than those of the Nafion112 membrane.

For the Nafion-based PEMs, the rate of gas permeation is proportional to the product of a permeability coefficient and a partial pressure and inversely proportional to the membrane thickness. It has been established that oxygen permeates through the hydrophobic part of the membrane and hydrogen diffuses through the ion clusters of membrane.[39] Owing to larger amount of hydrophobic PTFE component and the thinness of the PTFE-reinforced membranes, Pt−SiO_2/NP and NP membranes show almost twice the oxygen and hydrogen permeability as compared to those of Nafion112, although the thickness values of the former are only 40% that of the latter. In Table 2, the oxygen permeability of the Nafion112 membrane is 0.25×10^{-9} $m^3 \cdot m \cdot m^{-2} \cdot s^{-1} \cdot MPa^{-1}$, which is consistent with 0.16×10^{-9}

TABLE 1: Comparison of Total/Bulk/Bound Water Content of the Nafion 112, Pt−SiO_2/NP, and NP Membranes

			λ_{H_2O/SO_3H}			$\Delta W_{H_20/dry-memb} \times 100$		
membrane type	EW/g·mol^{-1}	thickness/μm	total	bulk	bound	total	bulk	bound
Nafion112	1100	50	18.5	18.0	0.5	30.3	29.5	0.8
NP	1300	20	17.7	17.3	0.4	24.5	23.9	0.6
Pt−SiO_2/NP	1337	20	40.5	39.6	0.9	54.5	53.3	1.2

TABLE 2: Comparison of Mechanical Strength, Dimensional Stability and O_2 and H_2 Permeability Properties of Membranes

				reactants permeability × 10^9 (m^3·m·m^{-2}·s^{-1}·MPa^{-1}) at 80 °C		
membrane type	thickness/μm	max strength/MPa	break strength/MPa	O_2	H_2	dimensional change (%)
Nafion112	50	21.82	20.12	0.25	1.10	30
NP	20	38.12	36.64	0.44	2.14	7.50
Pt−SiO_2/NP	20	35.30	34.81	0.48	2.20	8.33

m^3·m·m^{-2}·s^{-1}·MPa^{-1} reported in ref 44. The hydrogen permeability and oxygen permeability of Pt−SiO_2/NP membrane are very close to those of the NP membrane.

From the above measurements, the ultrathin Pt−SiO_2/NP and NP membranes have improved mechanical properties, enhanced dimension stability, and acceptable hydrogen and oxygen permeability. This allows our ultrathin Pt−SiO_2/NP membrane to be considered for application in PEM fuel cells.

3.3. Experimental Analysis of the Membrane Self-Humidification Effect. The distribution profiles of the specific resistance (ρ) along the cross section measured by Pt probes inserted into membranes have a great advantage of in situ investigation of the self-humidification function of a membrane (60−80 μm) under dry operation.[29] However, it could not be applied in our membrane since the membrane is very thin (20 μm). Therefore, the single cell performance evaluations (see section 3.3.1), the areal resistance analyses of the operating membranes measured by EIS (see section 3.3.2), and the experiment of the collected water in the outlets of both anode and cathode by ice trap (see section 3.3.3) were combined to investigate and identify the self-humidification effect of Pt−SiO_2/NP membrane under dry operation.

3.3.1. Single PEM Fuel Cell Evaluation. Figure 7 shows the performances of a single cell employing the Pt−SiO_2/NP membrane with dry H_2/O_2 at $T_{cell} = 50$, 60, and 70 °C and with fully humidified H_2/O_2 at $T_{H_2} = T_{cell} = T_{O_2} = 60$ °C. The gas pressure is 0.20 MPa, and the hydrogen and oxygen stoichiometries are $\lambda_{H_2} = 1.1$ and $\lambda_{O_2} = 2.0$. The cell performance improves with the cell temperature ranging from 50 to 60 °C due to the enhanced kinetics of the cell reaction and proton transport. However, the optimum temperature for the Pt−SiO_2/NP membrane under dry H_2/O_2 operation is 60 °C, corresponding to the optimal temperature for the Nafion-based self-humidifying membrane under dry operation.[33] This is because water loss due to vaporization becomes more serious at higher temperature (70 °C), resulting in a dehydration of the MEA and a decrease in cell performance. The peak power densities of the fuel cells employing the Pt−SiO_2/NP membrane under wet and dry operation are 1.5 and 1.4 W cm^{-2}, respectively, indicating a slightly better performance of the Pt−SiO_2/NP membrane with fully humidified H_2/O_2 than that with dry H_2/O_2.

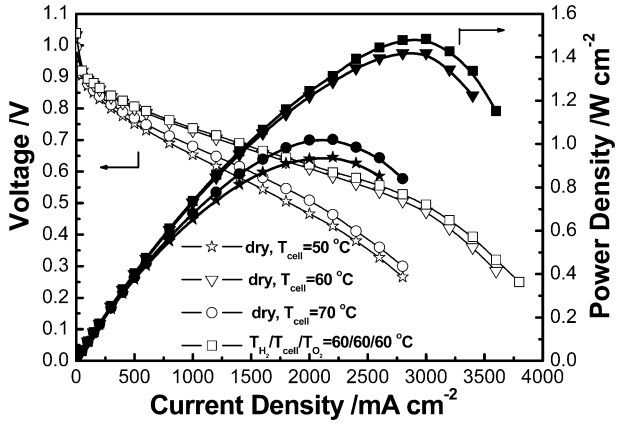

Figure 7. Performance comparison of single cell employing Pt−SiO_2/NP membrane with dry H_2/O_2 at 50 °C (☆, ★), 60 °C (▽, ▼), 70 °C (○, ●), and with fully humidified H_2/O_2 at $T_{H_2}/T_{cell}/T_{O_2}$ = 60/60/60 °C (□, ■). $P_{H_2} = P_{O_2} = 0.20$ MPa, $\lambda_{H_2} = 1.1$, $\lambda_{O_2} = 2.0$, $d_m = 20$ μm.

Figure 8 shows the performances of the single cells employing the Pt−SiO_2/NP membrane and the NP membrane with dry H_2/O_2 at $T_{cell} = 60$ °C, $P_{H_2} = P_{O_2} = 0.20$ MPa, and $\lambda_{H_2} = 1.1$ and $\lambda_{O_2} = 2.0$. As indicated in the figure, the cell employing the Pt−SiO_2/NP membrane outperforms that of the NP membrane at all recorded current densities. For example, the cell voltage at 2500 mA/cm^2 for the Pt−SiO_2/NP membrane is 0.55 V, which is 1.5 times relative to 0.36 V for the NP membrane. The peak power density values for the Pt−SiO_2/NP membrane and the NP membrane are 1.40 and 0.98 W cm^{-2}, respectively. This is attributed to hygroscopic Pt−SiO_2 particles in the membrane, which adsorbs water at low current density and releases water at high current density to satisfy the requirement of electro-osmotic drag.

Figure 9 shows the schematic diagrams of reactant gas crossover along MEA direction for Pt−SiO_2/NP and NP membranes under self-humidification operation. For the NP membrane, the amounts of crossover gas in the anode and the cathode regions are the same as that in the membrane. However,

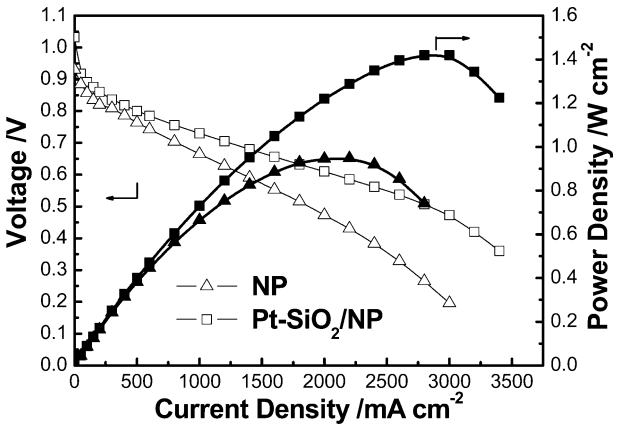

Figure 8. Performance comparison of single cell employing Pt−SiO_2/NP membrane (□, ■) and NP membrane (△, ▲) with dry H_2/O_2 at T_{cell} = 60 °C, $P_{H_2} = P_{O_2} = 0.20$ MPa, $\lambda_{H_2} = 1.1$, $\lambda_{O_2} = 2.0$, $d_m = 20$ μm.

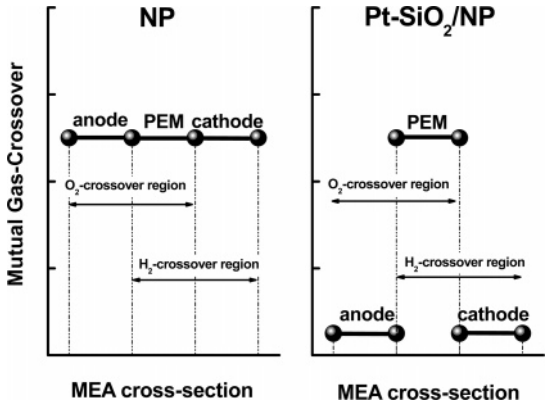

Figure 9. Schematic diagram of reactant gas crossover along the MEA direction for Pt−SiO_2/NP and NP membranes under self-humidification operation.

for the Pt−SiO_2/NP membrane, the amounts of crossover gas in the anode and the cathode regions are much less than that in the membrane region because the mutual gas crossover is chemically catalyzed into H_2O by Pt−SiO_2 catalyst inside the membrane. It is noteworthy that the cell OCV for the Pt−SiO_2/NP membrane under dry operation is 1.032 V, which is approximately 100 mV higher relative to that for the NP membrane (refer to Figure 8). As discussed in section 3.1, the crossover of the reactant gases was suppressed by the catalytic recombination at dispersed Pt inside the Pt−SiO_2/NP membrane, resulting in a higher value of OCV. It is thus clear that the crossover gas recombination significantly reduces mixed potential and cathode polarization in comparison with the plain NP membrane. Although the Pt loading inside the membrane is low (see section 3.2.1), duplicated fuel cell tests have shown that the effect of suppressing crossover gases in both the anode and the cathode was remarkable, which is in good agreement with the high cell OCV.

Therefore, the Pt−SiO_2/NP membrane showed similar cell performance between wet and dry operations (refer to Figure 7) and improved cell performance under dry operation relative to that of the NP membrane (refer to Figure 8). On the basis of the above fuel cell evaluations, the excellent self-humidification effect of the Pt−SiO_2/NP membrane was confirmed.

3.3.2. Resistance Measurement of the Membranes. To corroborate the surprisingly high single cell performance employing the Pt−SiO_2/NP membrane, the EIS measurement was employed to investigate the areal resistances of the membranes.

The areal resistance values of the single cells employing the Pt−SiO_2/NP membrane under dry and wet conditions and also that of the plain NP membrane under dry condition are obtained by EIS measurements. The conditions follow those in Figure 7 and Figure 8 except that the cell temperature is 60 °C. The areal resistance values for the Pt−SiO_2/NP membrane under wet and dry operations and for the NP membrane under dry operation are 0.19, 0.20, and 0.29 Ω·cm^2, respectively. The decreased areal resistance for the Pt−SiO_2/NP membrane under dry operation is ascribed to the hygroscopic property of the Pt−SiO_2 catalyst to keep higher water content (see section 3.2.2) and maintain better membrane water balance as compared to that of the NP membrane. The similar areal resistance values under dry operation and wet operation clearly demonstrate the self-humidification function of the Pt−SiO_2/NP membrane. These data sufficiently corroborate the excellent single cell performance of the Pt−SiO_2/NP membrane under self-humidification operation mode as compared to the NP membrane.

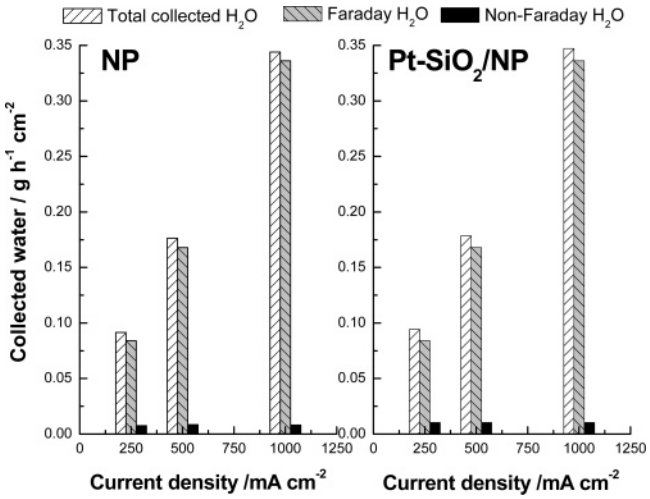

Figure 10. Comparison of the amounts of non-Faraday water and Faraday water for NP membrane and Pt−SiO_2/NP membrane under dry operation for 8 h at 250, 500, and 1000 mA/cm^2 of current density, respectively. $P_{H_2} = P_{O_2} = 0.02$ MPa, $T_{cell} = 60$ °C, $\lambda_{H_2} = 1.1$, $\lambda_{O_2} = 2.0$.

3.3.3. Water Collection at the Anode and the Cathode. 3.3.3.1. Amounts of Non-Faraday Water and Faraday Water. The non-Faraday water is generated by catalytic recombination of permeable H_2 and O_2. This type of water can be estimated by subtracting Faraday water (calculated from current density and operation time) from the total collected water in the ice trap.

Figure 10 compares the amounts of the non-Faraday water and the Faraday water for the Pt−SiO_2/NP and the NP membranes under dry operation at current densities of 250, 500, and 1000 mA/cm^2, $P_{H_2} = P_{O_2} = 0.02$ MPa, $T_{cell} = 60$ °C, and $\lambda_{H_2} = 1.1$ and $\lambda_{O_2} = 2.0$. The mass of water evaporated from the outlet in the ice trap (0 °C) can be estimated by supposing that the system of the ice trap is in saturation state at $T = 0$ °C ($P_{H_2O} = 0.006$ atm) with outlet H_2 and O_2 flowing for 8 h. Corresponding to the gas stoichiometries, the flow of the outlet H_2 and O_2 through the ice trap was 1.94 and 8.75 cm^3/min at 500 mA/cm^2. The amount of non-Faraday water was 0.42 g in 8 h, and calculations showed that the mass ratios of the evaporated water to the non-Faraday water were 1.1% and 4.8% for the H_2 and O_2 flows, respectively. It is thus clear that the amount of evaporated water at 0 °C in the ice trap was very small and negligible compared with that of the non-Faraday water.

Furthermore, for example, the ratio of the non-Faraday water to the Faraday water was 5.0% and 6.2%, respectively, for the NP and Pt−SiO_2/NP membranes when the cell was operated at 500 mA/cm^2. The amount of the non-Faraday water for the Pt−SiO_2/NP membrane is slightly higher than that for the NP membrane. Although the amount of the non-Faraday water is about 5% that of the Faraday water for both the membranes, there is an intrinsic difference between them. For the Pt−SiO_2/NP membrane, the non-Faraday water was in situ generated inside the membrane and could immediately hydrate the membrane to satisfy the electro-osmotic drag requirement. As for the NP membrane, however, the non-Faraday water was generated in the electrodes (outside the membrane) and could not hydrate the membrane.

Furthermore, the non-Faraday water in situ generated inside the Pt−SiO_2/NP membrane not only facilitates hydration of the membrane but also accelerates the water back-diffusion from the cathode to the anode. Thus, the non-Faraday water also

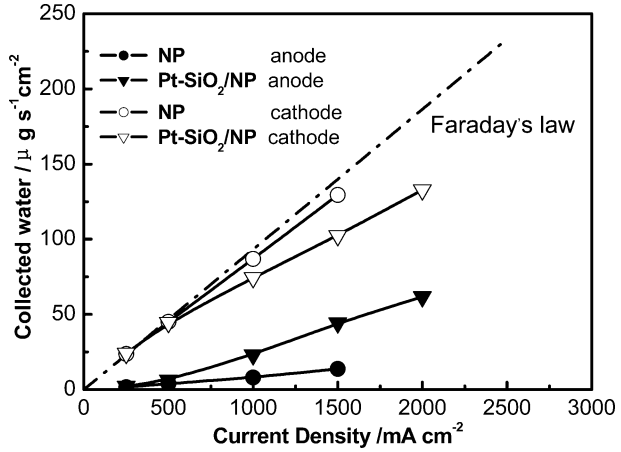

Figure 11. Comparison of the amount of collected water in anode and cathode for NP membrane and Pt−SiO_2/NP membrane under dry operation at various current densities. $P_{H_2} = P_{O_2} = 0.02$ MPa, $T_{cell} = 60$ °C, $\lambda_{H_2} = 1.1$, $\lambda_{O_2} = 2.0$.

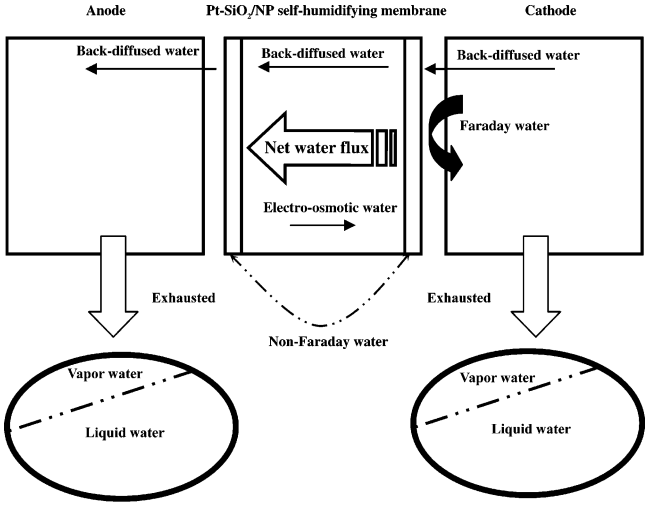

Figure 12. Water profile of Pt−SiO_2/NP membrane under dry operation.

contributes to the reduced areal resistance of the operating Pt−SiO_2/NP membrane measured by EIS (see section 3.3.2) and leads to significantly improved cell performance.

3.3.3.2. Net Water Drag from the Cathode to the Anode. Figure 11 compares the exhausted water at both the anode and the cathode for the NP membrane and the Pt−SiO_2/NP membrane under dry operation at current densities of 250, 500, 1000, 1500, and 2000 mA/cm^2, $P_{H_2} = P_{O_2} = 0.02$ MPa, $T_{cell} = 60$ °C, and gases stoichiometries of $\lambda_{H_2} = 1.1$ and $\lambda_{O_2} = 2.0$. For the Pt−SiO_2/NP membrane, the curves of collected water at the anode and the cathode as a function of current densities are much closer and imply better water balance across the operating PEM fuel cell, relative to those for the NP membrane. The more collected water at the anode accounts for the faster water back-diffusion from the cathode. It is deduced that for the purpose of comparison of Pt−SiO_2/NP and NP membranes, the higher the current density was, the more back-diffused water was needed from the cathode to satisfy electro-osmotic drag and thus the more remarkable self-humidification effect was observed. Therefore, it is reasonable that the current density was fixed at 1500 mA/cm^2 to investigate the reverse net water transport from the cathode to the anode.

Figure 12 shows the water profile for the Pt−SiO_2/NP membrane under dry operation. The water distribution across an operating PEM fuel cell using dry reactant gases depends on several parameters. On one hand, water is transported from the anode to the cathode across the membrane by electro-osmotic drag. On the other hand, the back-diffused water from the cathode to the anode is due to the concentration gradient. The concentration gradient is attributed to the transport of water by electro-osmotic drag and the water generated at the cathode by oxygen reduction reaction. The net water flux through the operating PEM fuel cell is the combined result of the electro-osmotic drag and the back-diffusion of water from the cathode to the anode.[19,20,36] The net water drag from the anode to the cathode under external-humidifying operation was predicted[35] and observed as 0.2 H_2O per proton.[19] However, the reverse one toward the anode was qualitatively deduced.[26,36] Interestingly, a reverse net water drag (from the cathode to the anode) is quantitatively found under our measurement conditions.

To calculate the reverse net water drag, the data of collected water at the anode and the cathode for the Pt−SiO_2/NP and the NP membranes at 1500 mA/cm^2 are derived from Figure 11. It is noteworthy that the 30% of total collected water discharged at the anode was obtained for the Pt−SiO_2/NP membrane with respect to 9% for the NP membrane. These values correspond to a flux of water of 221.4 and 68.9 μg/s for the 5 cm^2 cell, which is in accordance with 44.3 and 13.8 μg/s·cm^2, respectively. These measured values could be compared to the theoretical values based on the ex situ determination of D_{H_2O} ($D_{H_2O} = 4$ to 8×10^{-6} cm^2/s at 30 °C, depending to membrane hydration) in Nafion117 by Zawodzinski et al.[14,35,45] According to Fick's first law

$$\text{flux} = D_{H_2O}(dC_{H_2O}/dx) \quad (4)$$

Büchi et al.,[26] on the basis of assumption of $D_{H_2O} = 8 \times 10^{-6}$ cm^2/s, obtained that the theoretical water flux is 60 μg/s·cm^2 in Nafion117 at 200 mA/cm^2. This value is higher than our experimental values due to the theoretical assumption of maximum D_{H_2O}. Consequently, the high water flux discharged at the anode is within the theoretical limit. The reverse net water flux (toward the anode) of the Pt−SiO_2/NP membrane is almost 3.2 times that of the NP membrane, which is ascribed to its better membrane hydration reflected by higher water content. The net water drag across an operating fuel cell employing dry reactant gases could easily be calculated from the charge passed during the operation time and the water collected at the anode. The reverse net water drag toward the anode is 0.16 and 0.05 H_2O/H^+ for the Pt−SiO_2/NP and the NP membranes, respectively.

So it is deemed that for our Pt−SiO_2/NP membrane with optimized structure, the collected water at the anode derives from the accelerated water back-diffusion from the cathode. The reverse net water drag suggests that the back-diffused water could not only completely satisfy but also exceed the requirement of electro-osmotic drag. On the basis of the above-mentioned data, the fact of the reverse net water flux toward the anode suggests that the Pt−SiO_2/NP membrane exhibits much faster water back-diffusion and better water balance than the NP membrane. This results in an enhanced cell performance under dry operation.

4. Conclusions

An ultrathin PTFE-reinforced self-humidifying composite membrane with a sandwich structure was developed. The sandwich structure of the Pt−SiO_2/NP membrane is based on the consideration of accelerating water back-diffusion in the ultrathin membrane and of suppressing reactant gas permeation

resulting from the thin NP membrane. The nanometer-sized SiO_2-supported Pt catalyst inside the Pt−SiO_2/NP membrane contributes to the enhanced self-humidification at the anode side, decreased cathode polarization, and accordingly improved OCV.

The membrane structure was confirmed by TEM, ICP-AES, SEM, EDS, etc. The improved mechanical properties and the enhanced dimension stability due to PTFE reinforcement, and the acceptable hydrogen and oxygen permeability could allow ultrathin Pt−SiO_2/NP membrane for application in PEM fuel cells. Due to the existence of a hygroscopic Pt−SiO_2 catalyst, the Pt−SiO_2/NP membrane adsorbs almost twice the amount of total/bulk/bound water as compared to the NP membrane, which implies better water balance of the membrane.

The single cell employing the Pt−SiO_2/NP membrane under dry H_2/O_2 has a peak power density of 1.40 W cm^{-2} and a cell OCV of 1.032 V. The Pt−SiO_2/NP membrane outperforms the plain NP membrane and exhibits a higher cell OCV under dry operation mode. The performance of the single cell employing the Pt−SiO_2/NP membrane is slightly influenced by the humidification condition. The reduced areal resistance measured by EIS for the Pt−SiO_2/NP membrane under dry operation, with respect to that for the NP membrane, is attributed to hygroscopic Pt−SiO_2 catalyst inside the membrane.

Although the amount of the non-Faraday water is very small relative to the Faraday water, the non-Faraday water generated inside the Pt−SiO_2/NP membrane could effectively hydrate the membrane, and accelerate back diffusion of water and thus facilitate the water equilibrium as compared to that for the NP membrane. Interestingly, through the optimized Pt−SiO_2/NP membrane structure, a reverse net water drag (from cathode to anode) is quantitatively found to be 0.16 H_2O/H^+ under normal constant H_2 and O_2 stoichiometries ($\lambda_{H_2} = 1.1$ and $\lambda_{O_2} = 2$). This accounts for the accelerated back-diffused water to the anode, which could not only meet but also exceed the requirement of electro-osmotic drag.

Therefore, on the basis of fuel cell evaluations, EIS measurements, and collected water experiments, the excellent self-humidification performance of the Pt−SiO_2/NP membrane is corroborated. The excellent self-humidifying cell performance is of significance for quick start-up and abrupt load changes in the practical application of PEM fuel cells.

Acknowledgment. This work was supported by the National Natural Science Foundation of China (20476104).

References and Notes

(1) Steele, B. C. H.; Heinzel, A. *Nature* **2001**, *414*, 345.
(2) Savadogo, O. *J. New Mater. Electrochem. Syst.* **1998**, *1*, 47.
(3) Prater, K. B. *J. Power Sources* **1992**, *37*, 181.
(4) Appleby, A. J. *J. Power Sources* **1992**, *37*, 223.
(5) Srinivasan, S.; Manko, D. J.; Koch, H.; Enayetullah, M. A.; Appleby, A. J. *J. Power Sources* **1990**, *29*, 367.
(6) Eikerling, M.; Kornyshev, A. A.; Kuznetsov, A. M.; Ulstrup, J.; Walbran, S. *J. Phys. Chem. B* **2001**, *105*, 3646.
(7) Kornyshev, A. A.; Kuznetsov, A. M.; Spohr, E.; Ulstrup, J. *J. Phys. Chem. B* **2003**, *107*, 3351.
(8) Mathias, M. F.; Makharia, R.; Gasteiger, H. A.; Conley, J. J.; Fuller, T. J.; Gittleman, C. J.; Kocha, S. S.; Miller, D. P.; Mittelsteadt, C. K.; Xie, T.; Yan, S. G.; Yu, P. T. *Electrochem. Soc. Interface* **2005**, Fall, 24.
(9) Ioselevich, A. S.; Kornyshev, A. A.; Steinke, J. H. G. *J. Phys. Chem. B* **2004**, *108*, 11953.
(10) Pivovar, A. M.; Pivovar, B. S. *J. Phys. Chem. B* **2005**, *109*, 785.
(11) Kadirov, M. K.; Bosnjakovic, A.; Schlick, S. *J. Phys. Chem. B* **2005**, *109*, 7664.
(12) Saito, M.; Hayamizu, K.; Okada, T. *J. Phys. Chem. B* **2005**, *109*, 3112.
(13) Spohr, E.; Commer, P.; Kornyshev, A. A. *J. Phys. Chem. B* **2002**, *106*, 10560.
(14) Zawodzinski, T. A., Jr.; Springer, T. E.; Uribe, F.; Gottesfeld, S. *Solid State Ionics* **1993**, *60*, 199.
(15) Yeo, R. S. *J. Electrochem. Soc.* **1983**, *130*, 533.
(16) Hill, R.; Verbrugge, M. W. *J. Electrochem. Soc.* **1990**, *137*, 886.
(17) Bernardi, D. M. *J. Electrochem. Soc.* **1990**, *137*, 3344.
(18) Cappadonia, M.; Erning, J. W.; Saberi Niaki, S. M.; Stimming U. *Solid State Ionics.* **1995**, *77*, 65.
(19) Zawodzinski, T. A., Jr.; Derouin, C.; Radzinski, S.; Sherman, R. J.; Smith, V. T.; Springer, T. E.; Gottesfeld, S. *J. Electrochem. Soc.* **1993**, *140*, 1041.
(20) Fuller, T. F.; Newman, J. *J. Electrochem. Soc.* **1992**, *139*, 1332.
(21) Bernardi, D. M.; Verbrugge, M. W. *J. Electrochem. Soc.* **1992**, *139*, 2477.
(22) Savadogo, O. *J. Power Sources.* **2004**, *127*, 135.
(23) Ciureanu, M.; Badita, M. *J. New Mater. Electrochem. Syst.* **2003**, *6*, 163.
(24) Watanabe, M.; Satoh, Y.; Shimura, C. *J. Electrochem. Soc.* **1993**, *140*, 3190.
(25) Watanabe, M.; Sakairi, K.; Inoue, M. *J. Electroanal. Chem.* **1994**, *375*, 415.
(26) Büchi, F. N.; Srinivasan, S. *J. Electrochem. Soc.* **1997**, *144*, 2767.
(27) Watanabe, M.; Uchida, H.; Seki, Y.; Emori, M.; Stonehart P. *J. Electrochem. Soc.* **1996**, *143*, 3847.
(28) Watanabe, M.; Uchida, H.; Emori, M. *J. Electrochem. Soc.* **1998**, *145*, 1137.
(29) Watanabe, M.; Uchida, H.; Emori, M. *J. Phys. Chem. B* **1998**, *102*, 3129.
(30) Uchida, H.; Ueno, Y.; Hagihara, H.; Watanabe, M. *J. Electrochem. Soc.* **2003**, *150*, A57.
(31) Lee, H. K.; Kim, J. I.; Park, J. H.; Lee, T. H. *Electrochim. Acta* **2004**, *50*, 761.
(32) Xing, D. M.; Yi, B. L.; Fu, Y. Z.; Liu, F. Q.; Zhang, H. M. *Electrochem. Solid-State Lett.* **2004**, *7*, A315.
(33) Yang, B.; Fu, Y. Z.; Manthiram, A. *J. Power Sources* **2005**, *139*, 170.
(34) Liu, F. Q.; Yi, B. L.; Xing, D. M.; Yu, J. R.; Hou, Z. J.; Fu, Y. Z. *J. Power Sources* **2003**, *124*, 81.
(35) Springer, T. E.; Zawodzinski, T. A.; Gottesfeld, S. *J. Electrochem. Soc.* **1991**, *138*, 2334.
(36) Voss, H. H.; Wilkinson, D. P.; Pickup, P. G.; Johnson, M. C.; Basura, V. *Electrochim. Acta* **1995**, *40*, 321.
(37) Kaliaguine, S.; Mikhailenko, S. D.; Wang, K. P.; Xing, P.; Robertson, G.; Guiver, M. *Catal. Today* **2003**, *82*, 213.
(38) Bahar, B.; Hobson, A. R.; Kolde, J. A.; Zuckerbrod, D. U.S. Patent 5,547,551.
(39) Yoshitake, M.; Tamura, M.; Yoshida, N.; Ishisaki, T. *Denki Kagaku* **1996**, *64*, 727.
(40) Eikerling, M.; Kornyshev, A. A.; Stimming, U. *J. Phys. Chem. B* **1997**, 101, 10807.
(41) Watanabe, M.; Igarashi, H.; Yoshioka, K. *Electrochim. Acta* **1995**, *40*, 329.
(42) Mclean, R. S.; Doyle, M.; Sauer, B. B. *Macromolecules* **2000**, *33*, 6541.
(43) Kolde, J. A.; Bahar, B.; Wilson, M. S.; Zawodzinski, T. A.; Gottesfeld, S. In Proceedings of the First International Symposium on Proton Conducting Membrane Fuel Cells; Gottesfeld, S. Halpert, G., Landgrebe, A., Eds.; The Eletrochemical Society Proceedings Series; Electrochemical Society: Pennington, NJ, 1995; Vol. 95−23, pp 193−201.
(44) Xing, D. M.; Yi, B. L.; Liu, F. Q.; Zhang, H. M. *Fuel Cells* **2005**, *5*, 406.
(45) Zawodzinski, T. A., Jr.; Neeman, M.; Sillerud, L. O.; Gottesfeld, S. *J. Phys. Chem.* **1991**, *95*, 6040.